

Article

Oxidative Thermal Conversion of Hydrothermal Derived Precursors toward the Mixed-Metal Cobaltite Spinel Oxides (ZnCo_2O_4 and NiCo_2O_4): In-Situ Investigation by Synchrotron-Radiation XRD and XAS Techniques

Wanchai Deelod ¹, Yuranan Hanlumyung ², Wanwisa Limphirat ³, Songwut Suramitr ¹, Kantapat Chansaenpak ⁴, Pongsakorn Kanjanaboos ⁵, Suttipong Wannapaiboon ^{3,*} and Worawat Wattanathana ^{2,*}

¹ Department of Chemistry, Faculty of Science, Kasetsart University, Bangkok 10900, Thailand; Wanchai.de@ku.th (W.D.); fsciswsm@ku.ac.th (S.S.)

² Department of Materials Engineering, Faculty of Engineering, Kasetsart University, Bangkok 10900, Thailand; yuranan.h@ku.th

³ Synchrotron Light Research Institute, 111 University Avenue, Suranaree, Muang, Nakhon Ratchasima 30000, Thailand; wanwisa@slri.or.th

⁴ National Nanotechnology Center, National Science and Technology Development Agency, Thailand Science Park, Khlong Luang 12120, Thailand; kantapat.cha@nanotec.or.th

⁵ School of Materials Science and Innovation, Faculty of Science, Mahidol University, Nakhon Pathom 73170, Thailand; pongsakorn.kan@mahidol.edu

* Correspondence: suttipong@slri.or.th (S.W.); fengwwa@ku.ac.th (W.W.)



Citation: Deelod, W.; Hanlumyung, Y.; Limphirat, W.; Suramitr, S.; Chansaenpak, K.; Kanjanaboos, P.; Wannapaiboon, S.; Wattanathana, W. Oxidative Thermal Conversion of Hydrothermal Derived Precursors toward the Mixed-Metal Cobaltite Spinel Oxides (ZnCo_2O_4 and NiCo_2O_4): In-Situ Investigation by Synchrotron-Radiation XRD and XAS Techniques. *Crystals* **2021**, *11*, 1256. <https://doi.org/10.3390/cryst11101256>

Academic Editors: Jesús Prado-Gonjal, Beatriz Molero-Sánchez and Sara A. López-Paz

Received: 20 September 2021

Accepted: 13 October 2021

Published: 17 October 2021

Publisher's Note: MDPI stays neutral with regard to jurisdictional claims in published maps and institutional affiliations.



Copyright: © 2021 by the authors. Licensee MDPI, Basel, Switzerland. This article is an open access article distributed under the terms and conditions of the Creative Commons Attribution (CC BY) license (<https://creativecommons.org/licenses/by/4.0/>).

Abstract: In-situ investigations of structural transitions during the thermal-oxidative event of mixed-metal spinel oxide precursors, the so-called nickel- (NCO) and zinc-containing (ZCO) cobaltite spinel precursors, were investigated to understand the formations of the derived NiCo_2O_4 and ZnCo_2O_4 spinel oxides, respectively. In-situ XRD investigation revealed that emerged temperatures for spinel oxide phase were between 325 and 400 °C, depending on the cationic substituent. It indicated that the emerged temperature correlated with the absolute octahedral site preference energy (OSPE) of those cations that participated in the development of the spinel framework. Moreover, the incorporated nickel and zinc in the precursors was beneficial for inhibiting the occurrence of the undesired CoO phase. Time-resolved X-ray absorption spectroscopic (TRXAS) data suggested the local structure rearrangement of nickel and zinc throughout the calcination process, which differed from the behavior of single-metal cobalt system. The essential information reported herein provides a benefit to control the cationic distribution within spinel materials, leading to the tunable physical and chemical properties.

Keywords: cobaltite spinel; in-situ analysis; X-ray diffraction; time-resolved X-ray absorption spectroscopy

1. Introduction

Cobaltite spinel oxide (CoCo_2O_4 , or Co_3O_4) has gained great interest as a material with high potential for energy storage, magnetic, and chemical catalytic applications [1–3]. The distribution of Co^{2+} and Co^{3+} ions over the tetrahedral (T_d) and octahedral (O_h) spinel interstices is a key factor to deliver remarkable material properties for specific applications [2,4–7]. Moreover, the cobaltite spinel framework can accommodate other first-row transition metals (such as nickel, copper, and zinc) as the substituents, leading to a variety of mixed-metal spinel derivatives [8–12]. In this aspect, the ZnCo_2O_4 and NiCo_2O_4 mixed-metal spinels are the major derivatives of cobalt-based spinels. Both materials have significantly attracted extensive consideration in the energy storage field regarding their remarkable electrochemical activities [6,13–16]. Moreover, their excellent electrical properties are prime for the fabrication of organic–inorganic hybrid devices which have

gained considerable interest recently [17,18]. Therefore, a suitable synthesis condition which could lead to a production of high purity mixed-metal spinel oxides on a large scale is necessary to serve their future demand.

To obtain mixed-metal cobalt-based spinel oxides, the oxidative-thermal conversion of the designed precursor compound is a main approach [1,7,19]. Generally, an elevated temperature is required for the decomposition of the precursor and subsequently the metal-cationic diffusion to construct the crystalline spinel framework. As it is complementary, the mixed-metal spinel precursor synthesized by hydrothermal crystallization seems to be suitable for the thermal conversion approach. This method usually provides a great advantage for manipulating and fine tuning the molar stoichiometry of mixed transition metals within the homogeneous precursors [20–23]. Hence, the successful synthesis of various spinel compounds, including ZnCo_2O_4 and NiCo_2O_4 spinels, using the calcination of hydrothermal derived precursors has been reported [20,24,25]. Typically, the resultant ZnCo_2O_4 from the aforementioned method is obtained in the form of normal spinel structure, in which the incorporated Zn^{2+} substitutes the Co^{2+} in T_d site. Alternatingly, an inverse NiCo_2O_4 spinel compound results from the substitution of Co^{3+} in O_h site along with the incorporated Ni^{2+} . Therefore, investigating the formation and the role of the incorporated metals in ZnCo_2O_4 and NiCo_2O_4 in normal and inverse spinel structures, respectively, is a key essential step for further controlling the cationic distribution in a mixed-metal spinel. Nevertheless, the insight into the mechanistic understanding of the phase transformation of the hydrothermal-derived precursors during the thermal treatment remains scarce. The knowledge on this aspect would be beneficial for tailoring the target spinel materials to obtain the desired properties. Recently, Cook et al. reported a time-resolved powder X-ray diffraction study of cobalt gallate spinel, exhibiting the structural development during solvothermal crystallization [26]. Though a similar in-situ analysis of dense oxide materials is relatively infrequent, only some prominent works have been reported so far [27–29]. Besides, the insight from this type of study might give rise to a better understanding of other mixed-metal functional structures like layer-double-hydroxide (LDH) [30–32], perovskite [33,34], and other advanced materials for environmental and energy-related applications [35–41].

Therefore, this work focuses on investigating the detailed phase transformation during the thermal treatment of two crystalline mixed-metal hydrothermal-derived precursors, for the synthesis of ZnCo_2O_4 and NiCo_2O_4 spinel materials. To understand the phase transformation mechanism in the subsequent thermal-oxidative step, in-situ X-ray diffraction (XRD) and time-resolved X-ray absorption (TRXAS) techniques were employed [42,43]. These two techniques allow a direct assessment and visualization in both the alteration of long-range and short-range ordering regarding the gradual vanishing of the precursor phase and the emerging formation of a desired crystalline mixed-metal spinel phase [44]. This study discloses unprecedented insights into the dynamic conversion from the hydrothermal-derived precursor towards spinel products during the thermal decomposition process, which could pave the way to scale up for large-scale production.

2. Materials and Methods

2.1. Material Synthesis

The mixed-metal spinel precursors for the synthesis of NiCo_2O_4 and ZnCo_2O_4 spinel oxides (named as NCO and ZCO precursors, respectively) were prepared by the hydrothermal crystallization approach. The hydrothermal solution was generated by dissolving a stoichiometric amount of analytical grade Zinc(II) acetate dihydrate (Sigma-Aldrich, St. Louis, MO, USA), cobalt(II) acetate tetrahydrate (Thermo-Fisher Scientific, Waltham, MA, USA), nickel(II) nitrate hexahydrate (Sigma-Aldrich, St. Louis, MO, USA), and urea (Carlo Erba, Barcelona, Spain) in deionized water. The molar ratio of the substituent cations (Ni^{2+} and Zn^{2+}) to Co^{2+} to urea was controlled to be 1:2:3.33 in all cases. The solution was sealed in a Teflon-liner stainless steel autoclave considering the filled fraction of 0.5 of the total liner volumes. Then, the hydrothermal reaction was carried out at 180 °C for 12 h.

The pink precursor powder was filtered out, washed with deionized water and ethanol (Carlo Erba, Barcelona, Spain), and after that was dried at 60 °C overnight. In addition, a single-metal precursor for the synthesis of pristine CoCo_2O_4 spinel oxide (so-called CCO precursor) was also prepared using a similar methodology but the second-metal substituent content was replaced by cobalt(II) acetate tetrahydrate.

2.2. Phase Transformation Study

A phase transformation experiment was performed at the Synchrotron Light Research Institute (SLRI), Nakhon Ratchasima, Thailand. Transformation of the chemical crystalline phases during oxidative thermal decomposition was determined by in-situ synchrotron-based X-ray diffraction at Beamline 1.1 W (Multiple X-ray Techniques, MXT). The precursor powder was finely ground and then densely packed on a sample holder. The sample holder was placed into the domed hot stage heating equipment (DHS 1100, Anton Paar, Graz, Austria) and covered with the semi-circle graphite dome. The domed hot stage was fed with an air supply provided by the built-in airflow system for temperature control upon heating and cooling. A step-heating program was set and monitored by the control software for the heating experiment. The sample was subsequently heated, from 300 °C to 475 °C, with a step temperature of 25 °C, heating rate of 20 °C/min, and a holding period of 45 min for each step. Synchrotron-based X-ray diffractograms were acquired during the holding periods using a 1-dimensional strip detector (Mythen 4K, DECTRIS, Baden, Switzerland) covering the 2θ ranging from 11.5° to 45.3° in the meantime. Herein, the X-ray photon energy of 12.0 keV, corresponding to the wavelength of 1.0332 Å, was used. The d-spacing of the oxide product was calculated based on Bragg's equation [7].

A time-resolved X-ray absorption (TRXAS) experiment was performed at Beamline 2.2 (Bonn-SUT-SLRI) [44,45]. Si (220) bending crystal was utilized as an energy dispersive monochromator (EDM). The precursor powders were homogenized with boron nitride powder (spectroscopic grade, Sigma Aldrich, St. Louis, USA) by ball-milling twice (40 Hz, 15 min each). The homogenized mixture was pelletized ($\varnothing = 4$ mm) by a mold pressing method (at 10 bars) and sealed in an in-house designed gas-flow reactor [44,45]. The sample pellet was heated from room temperature up to 480 °C, using the controlled heating rate of 3 °C per minute and the supply of N_2 and O_2 gaseous mixture ($42.18 \text{ cm}^3 \cdot \text{s}^{-1}$). XAS spectra probed at cobalt, nickel, and zinc K-edges were collected in transmission mode by the position-sensitive detector (PSD). Snapshots of metal cation K-edge spectra at a specified temperature were taken (10 shots, 1 s each). Spectra merge and normalization was carried out in Athena software (Demeter 0.9.26, Iffeffit 1.2.12). Metallic foils (cobalt, nickel, and zinc) were utilized as the standard samples for the conversion of pixel to energy.

3. Results

In-situ XRD profiles in Figure 1 illustrate the transformation of the CCO precursor toward cobalt oxide product by the elevating temperature from room temperature (RT) toward 475 °C. As viewed from top to bottom of the plot, the diffractogram at $T = 325$ °C indicated an emerged oxide phase by the reflection peaks that can be assigned to the CoCo_2O_4 spinel phase. As indicated in Figure 1, the phase development of CoCo_2O_4 is more pronounced at elevated temperatures. In the meantime, the decreasing of the reflection peak at 21.7° is observed, which indicates the vanishing of the precursor phase. However, the thermal conversion of the CCO precursor did not yield pure CoCo_2O_4 spinel oxide because the crystalline impurity contributing to XRD peaks at 24.3°, 28.1°, and 40.2° is also found. Those peaks can be indexed to the (111), (200), and (220) reflection planes of cobalt(II) oxide (CoO) (PDF #00-048-1719), respectively.

For a better data visualization, the progress of phase transition at a specific temperature was calculated concerning the normalized peak area from the diffractogram. Specifically, the integrated area of the main reflection peak belonging to the precursor (21.7°), the CoCo_2O_4 spinel (24.5°), and the CoO phases (28.1°) are considered. Note that the maximum intensity for each phase is considered as the reference point. Through this, the peak

intensity profiles, as shown in Figure 2, indicate the evolution of crystalline oxide phases at specific temperatures.

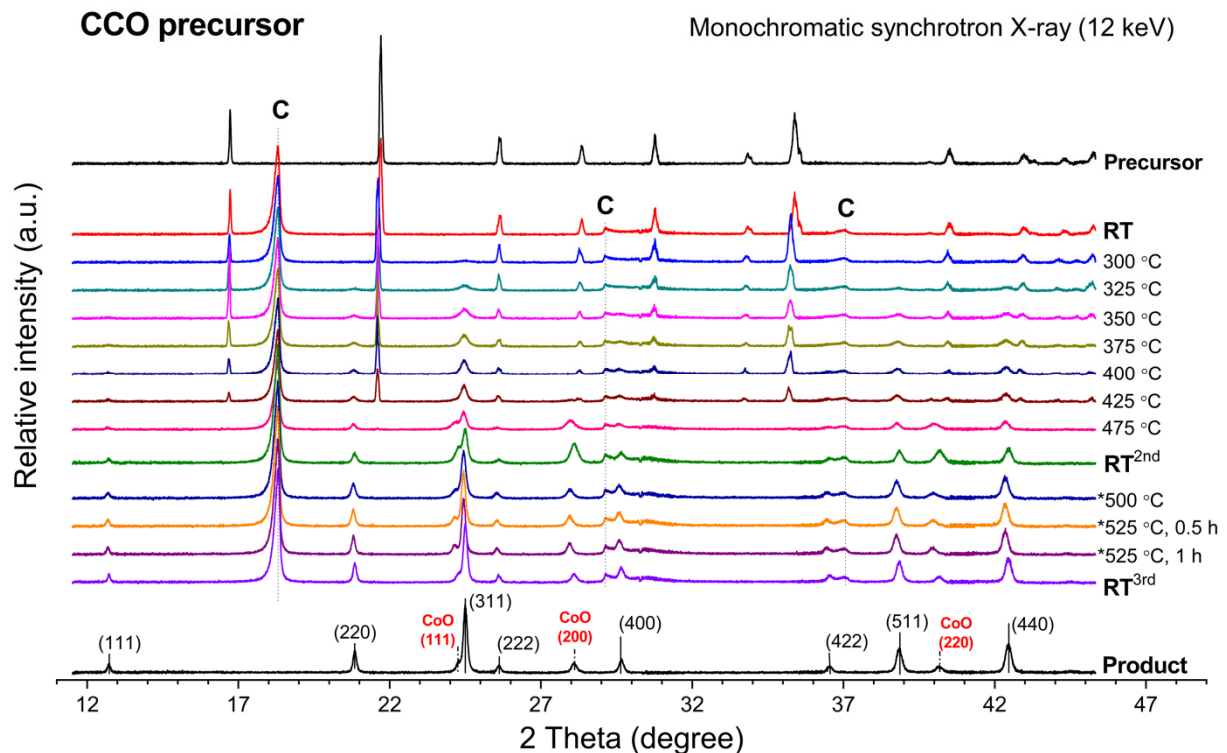


Figure 1. In-situ XRD profile representing phase transformation of the CCO precursor upon an elevating calcination temperature. (C = graphite dome, * = 2nd calcination cycle).

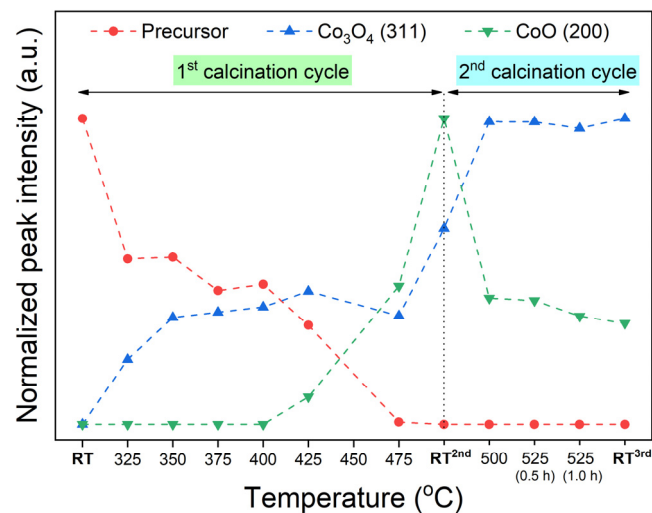


Figure 2. A profile of normalized XRD intensities, deriving from in-situ XRD data (Figure 1), represents the progress of phase transformation of the CCO precursor by elevating calcination temperature.

Apparently, with increasing temperature toward 475 °C, the existence of the precursor phase is gradually vanished, which consequently yields mixed-phase cobalt-based oxide products between CoO and CoCo_2O_4 . The CoCo_2O_4 spinel phase firstly forms at 325 °C, while the CoO phase emerges at 425 °C and higher. The CoO/ CoCo_2O_4 mixture gains more crystallinities along with heating the sample toward 475 °C. Moreover, the crystallinities of CoO and CoCo_2O_4 are significantly improved by the cooling down step, as evidenced by the increased peak intensity. As seen by comparing the XRD diffractograms at 475 °C

and at RT^{2nd} in Figure 1, a slight peak shift towards higher 2θ is observed, determining the lattice contraction after a cooling down process. The lattice spacing of each oxide compound at room temperature is examined (see Table S1 in Supplementary Materials).

The contribution of the CoO phase might come from two plausible reasons: (i) insufficient oxygen supply in the reaction chamber and (ii) degradation of CoCo_2O_4 oxide during the exposure to high temperatures. To clarify this, an additional calcination without any modification of the resulting sample was performed. By heating the sample to 525 °C and holding for 60 min, it was possible to reclaim the CoCo_2O_4 content from the CoO phase (Figure 1), but it required a longer time to obtain pure spinel oxide product. Additionally, pure CoCo_2O_4 spinel oxide was successfully produced by a separate calcination of the CCO precursor at 480 °C for 10 h (Figure S1). According to the result, the emerged CoO phase was considered as a metastable oxide phase of cobalt species deriving from insufficient oxygen content in the reaction chamber. It is noteworthy that the oxygen diffusion in bulk matrix of the precursor sample plays a crucial role in achieving high purity CoCo_2O_4 . The calcination temperature, time, and environmental oxygen content within the heating chamber are the essential factors to be optimized.

Apart from the CCO precursor, it is interesting to observe the influence of nickel and zinc incorporation on the phase transformation of the NCO and ZCO precursors. Since all in-situ XRD experiments were performed using a similar instrumental setup, all the differences from thermal conversion should solely originate from the effects of the second metal substituents. The in-situ XRD profiles in Figure 3, as well as the corresponding profiles of normalized peak intensity in Figure 4, demonstrate the progress of phase conversion of the ZCO and NCO precursors. For the ZCO precursor, Figures 3a and 4a indicate that the temperature of at least 325 °C is required for the emerged ZnCo_2O_4 spinel phase, which is similar to the case of CCO precursor. Moreover, the incorporated zinc content facilitates the precursor consumption rate due to an early disappearance of the crystalline ZCO precursor peak at 400 °C. Thermal conversion of the precursor directly yields pure ZnCo_2O_4 spinel, of which the lattice spacings are shown in Table S2.

In contrast, the NiCo_2O_4 spinel oxide is firstly formed by thermal conversion of the NCO precursor at 375 °C (Figures 3b and 4b), which is 50 °C higher than the required temperature for the emerging of CoCo_2O_4 and ZnCo_2O_4 spinel phases mentioned above. Thermal conversion of the as-prepared NCO precursor yields a phase-pure NiCo_2O_4 spinel oxide product, of which the lattice spacings are listed in Table S3. Furthermore, the crystalline NCO precursor phase exists at higher temperatures than the ZCO precursor, showing the vanishing temperature of 475 °C, similar to that of the CCO precursor. TEM images for the ZnCo_2O_4 and NiCo_2O_4 spinels prepared by calcining the ZCO and NCO precursor at 480 °C for 10 h are shown in Figure S2.

Investigation on the transition-metal K-edge by TRXAS illustrates the transformation of short-range ordering of each metal species participating in mixed-metal spinel oxide structure. TRXAS spectra in Figure 5 demonstrate the transformation progress of the local structure of cobalt and substituents in each precursor and/or the obtained products. The K-edge positions of cobalt and nickel (Figure 5a,c,d) slightly shift towards higher photon energy upon heating to the elevating temperatures, suggesting a higher contribution of trivalent species, i.e., Co^{3+} and Ni^{3+} , in the resulting spinel oxide compounds similar to previous reports [1,4–6,46]. However, due to the lack of an adequate energy calibration curve to examine nickel valency state precisely, all nickel cations in the obtained NiCo_2O_4 will be presumed as Ni^{2+} hereafter. Besides this, Zn^{2+} cation should participate in the ZnCo_2O_4 spinel regardless of the K-edge shift of ca. 0.6 eV (Figure 5b) [47].

Analysis of TRXAS spectra in the EXAFS region as shown in Figure 5 reveals a significant transformation of the local structure. Fourier transform (FT) of the EXAFS region into R-space implies the photoelectron scattering paths colliding with the neighbor coordinated atoms. The alteration of radial distance distribution around the probed element as illustrated in Figure 6 suggests the atomic repositioning in the perimeter nearby the probing element during an elevating calcination temperature.

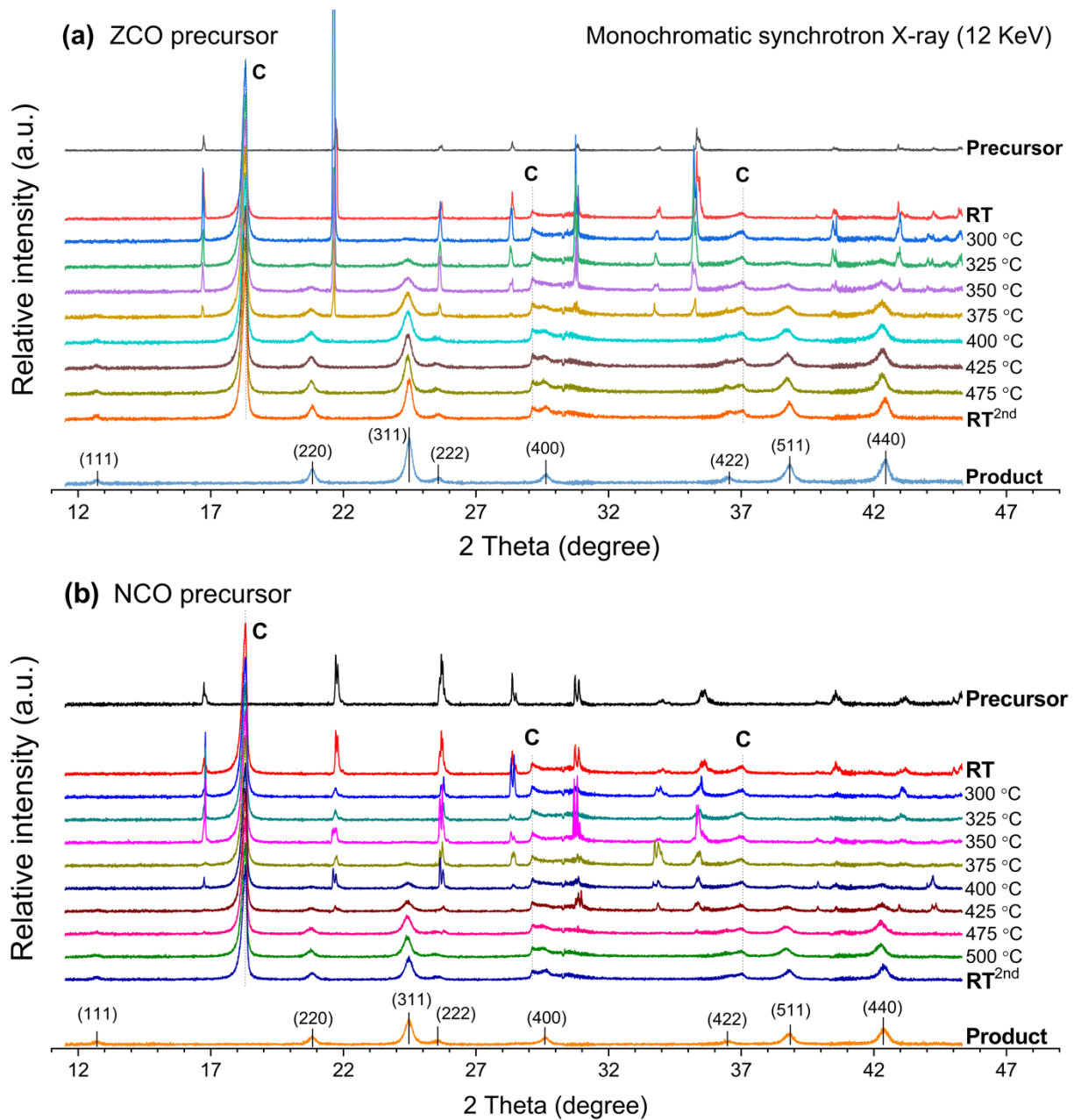


Figure 3. In-situ XRD profile represents phase transformation of the (a) ZCO precursor and (b) NCO precursor upon an elevating calcination temperature. (C = graphite dome).

It should be noted that the interatomic radial distance, which is mentioned hereafter, contained some level of uncertainty. Nevertheless, the variation of the radial distance distribution and magnitude is still reliable because the sample is investigated in-situ on an identical sample area.

As viewed from Figure 6a,c (from the bottom to the top), the development of the cobalt local structure can be roughly divided into two stages: (i) the establishment of the cobaltite spinel oxide structure during temperature ramping up and (ii) the maintenance of the established structure during the cooling down step. At the first stage, the local structure of cobalt is dramatically changed by the elevating temperature up to 480 °C. Afterward, that developed structure remains unchanged during the cooldown, suggesting a settlement of the cobaltite spinel framework. The first coordination shell of cobalt (after cooling down) is approximated to be around 1.35–1.36 Å for both the obtained products from thermal decomposition of the ZCO and NCO precursors. These estimated bond lengths are close

to the reported Co-O bond length in CoCo_2O_4 ($\sim 1.5 \text{ \AA}$) [48]. However, by using the same analogy as cobalt, different behaviors of the metal substituent can be found by focusing on the cooling down period. It is found that, after the settlement of the cobaltite spinel framework, the local environment of the substituents is drastically changed during the cooling down period. Therefore, the result indicates the repositioning of metal cationic substituents to approach the most stable occupation site during the cooling down step.

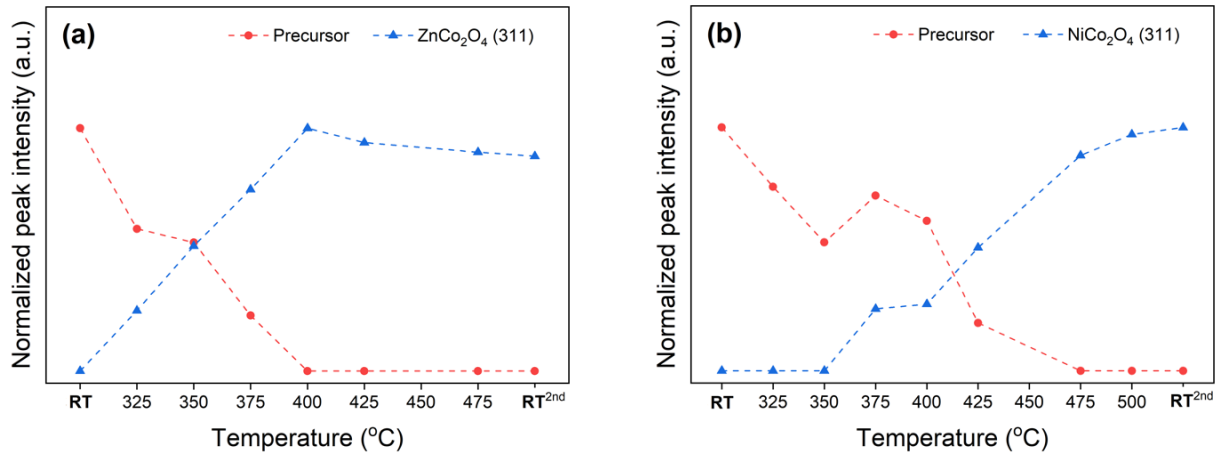


Figure 4. Profiles of normalized XRD intensities represent the progress of phase transformation of (a) ZCO and (b) NCO precursors, deriving from in-situ XRD data in Figure 3a,b, respectively.

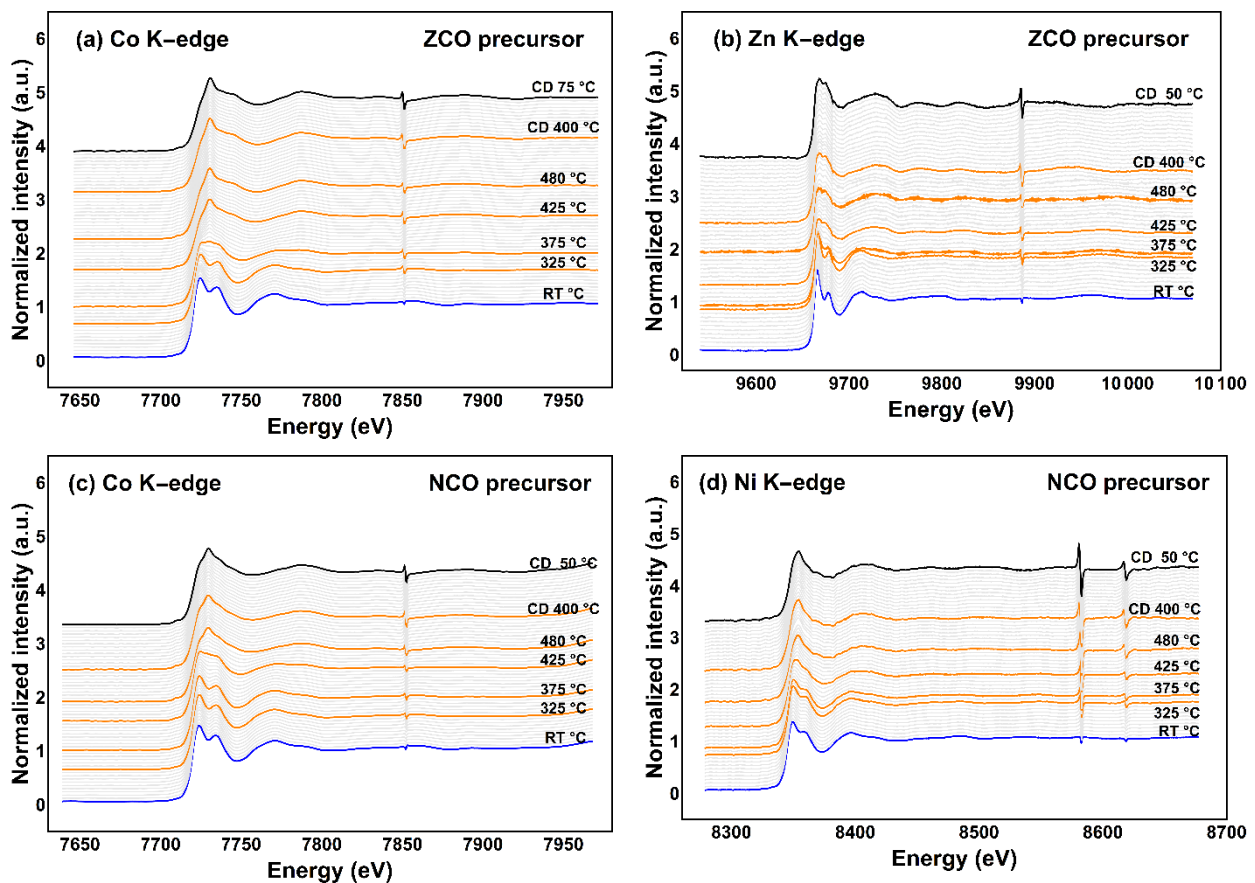


Figure 5. TRXAS K-edge spectra of metal species in two different spinel precursors; (a) cobalt and (b) zinc in the ZCO precursor; (c) cobalt, and (d) nickel in the NCO precursor.

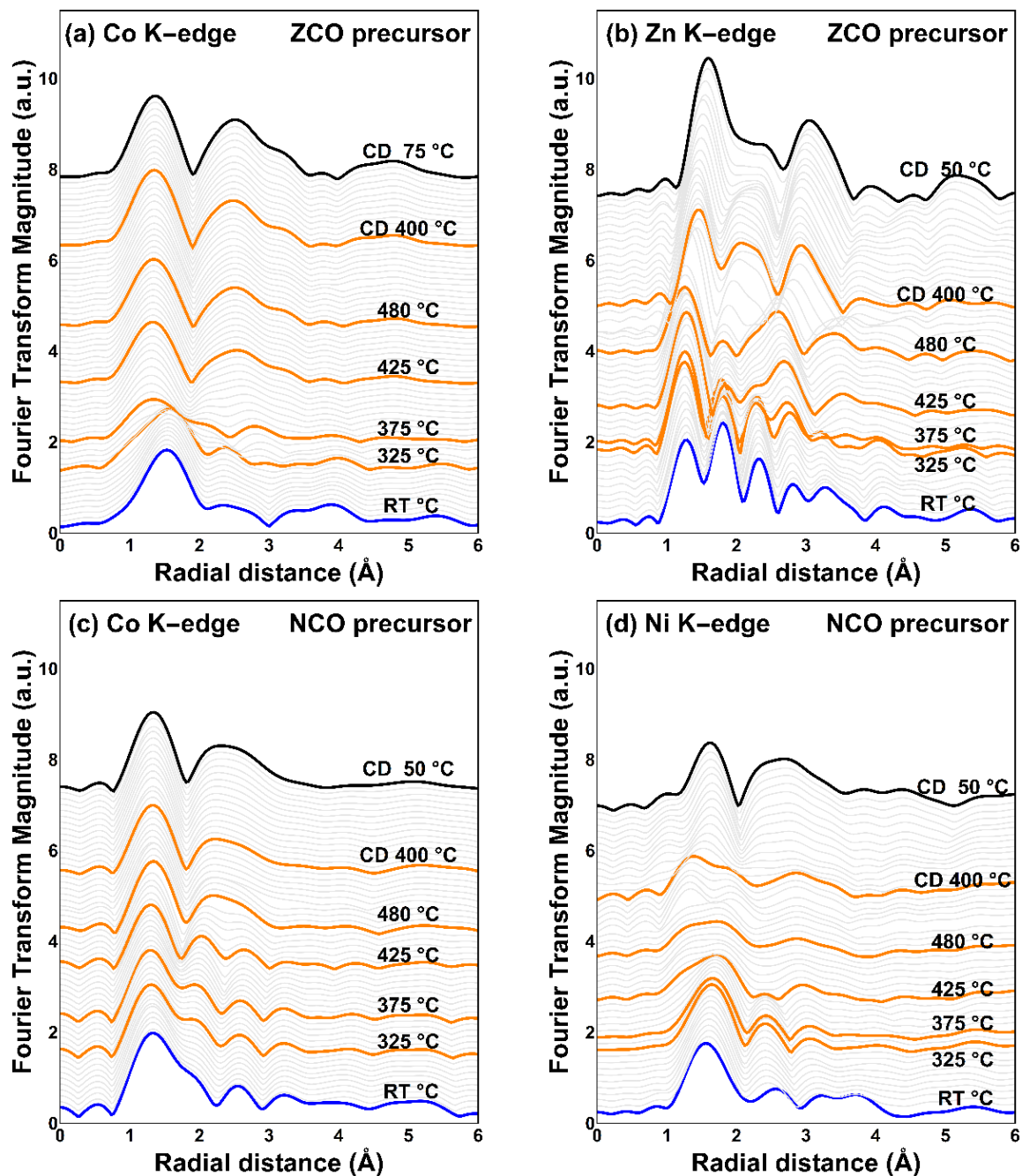


Figure 6. Fourier transform of TRXAS K-edge EXAFS region of metals in two different spinel precursors; (a) cobalt and (b) zinc in the ZCO precursor; (c) cobalt, and (d) nickel in the NCO precursor.

4. Discussion

The occurrence of pure ZnCo_2O_4 and NiCo_2O_4 spinel oxides from thermal conversion of their corresponding mixed-metal spinel precursors indicates a reliable synthesis method as described. CoCo_2O_4 is widely known as normal-spinel in which Co^{2+} occupies the T_d site while Co^{3+} is at the O_h site [49,50]. The normal-spinel formula of CoCo_2O_4 can be clarified as $\text{Co}^{2+}(\text{Co}_2^{3+})\text{O}_4$. The notation of the cationic species outside the parenthesis of the chemical formula indicates its occupancy in the T_d site. Meanwhile, the ZnCo_2O_4 is also known as another normal-spinel which can also be represented by $\text{Zn}^{2+}(\text{Co}_2^{3+})\text{O}_4$. According to in-situ XRD results, both normal spinels required similar temperatures, i.e., 325 °C (Figures 2 and 4a) for the crystalline phase formation. On the other hand, the NiCo_2O_4 , known as inverse-spinel represented by $\text{Co}^{3+}(\text{Ni}^{2+}\text{Co}^{3+})\text{O}_4$, emerged at a

higher temperature, i.e., 375 °C (Figure 4b). The emerging temperature for ZnCo_2O_4 and NiCo_2O_4 spinels is in a good agreement to the required temperature reported by other studies [19,24]. Furthermore, our study is in agreement with one from Johnsen and Norby, suggesting that the incorporated Zn^{2+} content helps the crystalline spinel to form at a lower temperature [51]. The significantly larger ionic radius Zn^{2+} readily occupies T_d site, as the elevated temperature gradually enlarges the site. In the opposite manner, NiCo_2O_4 spinel formation could be hindered by relatively similar cationic radii of nickel and cobalt ions.

We hypothesize that the emerging temperature for such cobaltite spinels should correlate with the preference of Co^{3+} to the O_h site, which is affected by the type of incorporated element. According to the literature, the preference of metal cation over the O_h site can be explained by the octahedral site preference energy (OSPE) [3]. The higher the absolute OSPE, the higher the tendency is for that cation to occupy the O_h site. It was reported that the absolute OSPE of Co^{3+} ($79.5 \text{ kJ}\cdot\text{mol}^{-1}$), which was far greater than that of the Co^{2+} ($31.0 \text{ kJ}\cdot\text{mol}^{-1}$) and the Zn^{2+} ($0 \text{ kJ}\cdot\text{mol}^{-1}$) [3]. Meanwhile, the absolute OSPE of Ni^{2+} ($86.2 \text{ kJ}\cdot\text{mol}^{-1}$) was slightly higher than that of Co^{3+} ($79.5 \text{ kJ}\cdot\text{mol}^{-1}$) [3]. Therefore, a similar emerging temperature for ZnCo_2O_4 and CoCo_2O_4 spinels is obtained, as by Zn^{2+} does not hinder the participation of Co^{3+} in the O_h site. On the other hand, the incorporated Ni^{2+} preferentially takes the O_h site and likely forces half of the Co^{3+} content to occupy the T_d interstice, which is the unstable site for Co^{3+} species. The repositioning of Co^{3+} toward the T_d site takes more energy for structural reordering and therefore results in a relatively higher temperature for the crystalline NiCo_2O_4 inverse spinel to be established.

As a consequence, the formation of spinel compounds in this study is more consistent with a pseudomartensitic type mechanism, as proposed by Chen et al., at which the oxygen anion establishes the spinel framework without delay (martensitic mechanism), and the metal cation takes a longer time to diffuse toward their respective spinel sites (diffusional mechanism) [29]. The role of oxygen can be seen by the early appearance of the X-ray diffracted peak that is mainly contributed by oxygen, i.e., (440) peak, in the diffractogram [52]. In the meantime, TRXAS provides the result regarding the diffusion behavior for short-range structure reordering of every metal cation along the elevating temperature.

In this particular instance, the different behavior between cobalt and substituent cations is illustrated by TRXAS through the change of short-range ordered structure in different time scales. It is found that the local structure of cobalt species are varied along with the heating up process and then settled, indicating the stable local environment after establishing the cobaltite spinel framework. In the meantime, repositioning of the substituent local environment is also observed as well. However, during the cooling down step, from 480 °C down to 50 °C, it seems that the local structure of cobalt remains unchanged (Figure 6a,c). In contrast, the reordering of substituent local structure is continued (Figure 6b,d). As evidence, the diffusion of substituents is confirmed to be rather delayed than that of the host cation. Therefore, it might be concluded that the heating up process is crucial for the decomposition of precursor and the establishing of cobaltite spinel framework. However, the cooling down step is also an essential period for the substituents to reposition themselves to be associated with the pre-constructed spinel framework. This information would be essential to design the synthesis procedure for tailoring the mixed-metal oxide with desired properties.

Apart from this, the incorporated zinc content stimulates the precursor consumption rate while the incorporated nickel content exhibits the reversed fashion. It underlines a different role of nickel and zinc associated with the cobaltite spinel establishment. Both nickel and zinc incorporations can prevent the formation of the CoO phase during thermal conversion. A plausible reason for that might be connected to the supply of divalent species by the substituent, Zn^{2+} and Ni^{2+} . With the lack of Co^{2+} in the heated sample, the CoO species cannot form, resulting in pure ZnCo_2O_4 and NiCo_2O_4 as the final products.

5. Conclusions

In this work, the interesting information concerning structural and phase transformation for nickel- (NCO), zinc-containing (ZCO), and undoped cobaltite spinel precursors (CCO) along the thermal-oxidative conversion was revealed by in-situ XRD and TRXAS techniques. The oxidative thermal conversion of the CCO precursor yields an impurity phase, CoO, which is co-developed and can partially be removed by re-calcining the impure product. However, the presence of nickel and zinc in the spinel precursors suppresses the formation of the crystalline-impurity CoO phase and consequently enhances the formation of the desired phase-pure spinel products. The threshold temperatures to yield the normal-spinel compounds, CoCo_2O_4 (from CCO precursor) and ZnCo_2O_4 (from ZCO precursor) are rather similar, at 325 °C. Meanwhile, the emerged inverse-spinel compound, NiCo_2O_4 (from NCO precursor), could be obtained at a higher temperature of at least 375 °C. The inverse-spinel compound requires a higher temperature to form a spinel framework because the substituent (Ni^{2+}) and host (Co^{3+}) cation compete to get over the same occupation site, namely the O_h site. Time-resolved X-ray absorption spectroscopy provides clues on the rearrangement of the Co, Ni, and Zn cationic occupancies. The result depicts the role of host cation (Co^{3+}) in establishing a cobaltite spinel framework during the heating step. After that, the local structure of cobalt seems to be stable, implying a non-significant change during the cooling down step. In contrast, the local structure of the substituent cations significantly changes during the cooling down step, which indicates the atomic repositioning to reach the most stable occupancy site. The emerging temperature of the spinel compound seems correlated with the absolute OSPE value of host and substituent. This essential information might be beneficial for wisely predicting the synthesis conditions to obtain pure mixed-metal cobaltite spinels with desired chemical compositions and properties. With expanding interest in ZnCo_2O_4 and NiCo_2O_4 mixed-metal spinel utilization in energy storage devices along with organic–inorganic hybrid devices for catalysis and biomedical purposes, the insight from this work which identifies a mechanism pathway and proper synthesis conditions could help open the door for production of high purity mixed-metal spinel oxides on a large scale for future usage.

Supplementary Materials: The following are available online at <https://www.mdpi.com/article/10.3390/cryst11101256/s1>; Figure S1: XRD profile of CoCo_2O_4 spinel oxide sample prepared by calcination of the CCO precursor at 480 °C, 10 hours, under air atmosphere (heating rate = 1 °C·min⁻¹), Figure S2: TEM images of the (a,c) ZnCo_2O_4 and (b,d) NiCo_2O_4 spinel oxides obtained by field-emission transmission electron microscope (FETEM, JEOL-JEM-3100F, operating voltage = 300 kV). The spinel oxide sample was prepared by calcining the prepared hydrothermal derived ZCO and NCO precursors at 480 °C in muffle furnace, under air flow for 10 hours (heating rate = 1 °C·min⁻¹), Table S1: XRD peak positions of the obtained product (at room temperature) after the thermal conversion of the CCO precursor, Table S2: XRD peak positions of the obtained product (at room temperature) after the thermal conversion of the ZCO precursor, Table S3: XRD peak positions of the obtained product (at room temperature) after the thermal conversion of the NCO precursor.

Author Contributions: Conceptualization, W.D., S.W. and W.W.; methodology, W.D., W.L., S.W. and W.W.; software, W.L.; validation, W.D., W.L., S.W. and W.W.; formal analysis, W.D., W.L., S.W. and W.W.; investigation, W.D., W.L., S.W. and W.W.; resources, Y.H., W.L., S.S., K.C., P.K., S.W. and W.W.; data curation, W.D., Y.H., W.L., S.W. and W.W.; writing—original draft preparation, W.D.; writing—review and editing, Y.H., P.K., S.W. and W.W.; visualization, W.D., Y.H., P.K., S.W. and W.W.; supervision, S.W. and W.W.; project administration, S.W. and W.W.; funding acquisition, P.K. and W.W. All authors have read and agreed to the published version of the manuscript.

Funding: This research received no external funding.

Data Availability Statement: The data presented in this study are available within the article and in Supplementary Materials.

Acknowledgments: Our deep appreciation is given to the Development and Promotion of Science and Technology Talents Project (DPST) scholarship for financial support. We thank the Center of Nanotechnology, Department of Chemistry, Kasetsart University, and the Department of Materials

Engineering, Kasetsart University, for crucial support for the research facilities and experimental venue. We acknowledge the Synchrotron Light Research Institute (Public Organization), SLRI, Thailand, for the provision of beamtime. All the staff from Beamline 1.1W (Multiple X-ray technique, MXT) and Beamline 2.2 Time-resolved XAS (Bonn-SUT-SLRI) are acknowledged for the experimental consulting, data interpretation, and assistance.

Conflicts of Interest: The authors declare no conflict of interest.

References

1. Dubal, D.; Gomez-Romero, P.; Sankapal, B.R.; Holze, R. Nickel cobaltite as an emerging material for supercapacitors: An overview. *Nano Energy* **2015**, *11*, 377–399. [[CrossRef](#)]
2. Wang, R.; Wu, J. 5—Structure and Basic Properties of Ternary Metal Oxides and Their Prospects for Application in Supercapacitors. In *Metal Oxides in Supercapacitors*; Dubal, D.P., Gomez-Romero, P., Eds.; Elsevier: Amsterdam, The Netherlands, 2017; pp. 99–132.
3. Ru, Q.; Zhao, D.; Guo, L.; Hu, S.; Hou, X. Three-dimensional rose-like ZnCo_2O_4 as a binder-free anode for sodium ion batteries. *J. Mater. Sci. Mater. Electron.* **2017**, *28*, 15451–15456. [[CrossRef](#)]
4. Loche, D.; Marras, C.; Carta, D.; Casula, M.F.; Mountjoy, G.; Corrias, A. Cation distribution and vacancies in nickel cobaltite. *Phys. Chem. Chem. Phys.* **2017**, *19*, 16775–16784. [[CrossRef](#)] [[PubMed](#)]
5. Marco, J.; Gancedo, J.; Gracia, M.; Gautier, J.; Ríos, E.; Berry, F. Characterization of the Nickel Cobaltite, NiCo_2O_4 , Prepared by Several Methods: An XRD, XANES, EXAFS, and XPS Study. *J. Solid State Chem.* **2000**, *153*, 74–81. [[CrossRef](#)]
6. Wu, Z.; Zhu, Y.; Ji, X. NiCo_2O_4 -based materials for electrochemical supercapacitors. *J. Mater. Chem. A* **2014**, *2*, 14759–14772. [[CrossRef](#)]
7. Smart, E.L.; Moore, E.A. *Solid State Chemistry: An Introduction*; Chapman & Hall: London, UK, 1995.
8. Zhu, J.; Gao, Q. Mesoporous MCo_2O_4 (M = Cu, Mn and Ni) spinels: Structural replication, characterization and catalytic application in CO oxidation. *Microporous Mesoporous Mater.* **2009**, *124*, 144–152. [[CrossRef](#)]
9. Naveen, A.N.; Selladurai, S. Tailoring structural, optical and magnetic properties of spinel type cobalt oxide (Co_3O_4) by manganese doping. *Phys. B Condens. Matter* **2015**, *457*, 251–262. [[CrossRef](#)]
10. Lakehal, A.; Benrabah, B.; Bouaza, A.; Dalache, C.; Hadj, B. Tuning of the physical properties by various transition metal doping in Co_3O_4 : TM (TM = Ni, Mn, Cu) thin films: A comparative study. *Chin. J. Phys.* **2018**, *56*, 1845–1852. [[CrossRef](#)]
11. Lakehal, A.; Bedhiah, B.; Bouaza, A.; Hadj, B.; Ammari, A.; Dalache, C. Structural, optical and electrical properties of Ni-doped Co_3O_4 prepared via Sol-Gel technique. *Mater. Res.* **2018**, *21*. [[CrossRef](#)]
12. Paudel, T.R.; Zakutayev, A.; Lany, S.; D’Avezac, M.; Zunger, A. Doping Rules and Doping Prototypes in A_2BO_4 Spinel Oxides. *Adv. Funct. Mater.* **2011**, *21*, 4493–4501. [[CrossRef](#)]
13. Li, Y.; Dai, H. Recent advances in zinc–air batteries. *Chem. Soc. Rev.* **2014**, *43*, 5257–5275. [[CrossRef](#)]
14. Hong, W.T.; Risch, M.; Stoerzinger, K.A.; Grimaud, A.; Suntivich, J.; Shao-Horn, Y. Toward the rational design of non-precious transition metal oxides for oxygen electrocatalysis. *Energy Environ. Sci.* **2015**, *8*, 1404–1427. [[CrossRef](#)]
15. Osgood, H.; Devaguptapu, S.V.; Xu, H.; Cho, J.; Wu, G. Transition metal (Fe, Co, Ni, and Mn) oxides for oxygen reduction and evolution bifunctional catalysts in alkaline media. *Nano Today* **2016**, *11*, 601–625. [[CrossRef](#)]
16. Vij, V.; Sultan, S.; Harzandi, A.M.; Meena, A.; Tiwari, J.N.; Lee, W.-G.; Yoon, T.; Kim, K.S. Nickel-Based Electrocatalysts for Energy-Related Applications: Oxygen Reduction, Oxygen Evolution, and Hydrogen Evolution Reactions. *ACS Catal.* **2017**, *7*, 7196–7225. [[CrossRef](#)]
17. Al Zoubi, W.; Yoon, D.K.; Kim, Y.G.; Ko, Y.G. Fabrication of organic-inorganic hybrid materials on metal surface for optimizing electrochemical performance. *J. Colloid Interface Sci.* **2020**, *573*, 31–44. [[CrossRef](#)] [[PubMed](#)]
18. Al Zoubi, W.; Kamil, M.P.; Fatimah, S.; Nashrah, N.; Ko, Y.G. Recent advances in hybrid organic-inorganic materials with spatial architecture for state-of-the-art applications. *Prog. Mater. Sci.* **2020**, *112*, 100663. [[CrossRef](#)]
19. Cabo, M.; Pellicer, E.; Rossinyol, E.; Castell, O.; Surinñach, S.; Baroó, M.D. Mesoporous NiCo_2O_4 Spinel: Influence of Calcination Temperature over Phase Purity and Thermal Stability. *Cryst. Growth Des.* **2009**, *9*, 4814–4821. [[CrossRef](#)]
20. Ding, R.; Qi, L.; Jia, M.; Wang, H. Simple hydrothermal synthesis of mesoporous spinel NiCo_2O_4 nanoparticles and their catalytic behavior in CH_3OH electro-oxidation and H_2O_2 electro-reduction. *Catal. Sci. Technol.* **2013**, *3*, 3207–3215. [[CrossRef](#)]
21. Che, H.; Liu, A.; Zhang, X.; Mu, J.; Bai, Y.; Hou, J. Three-dimensional hierarchical ZnCo_2O_4 flower-like microspheres assembled from porous nanosheets: Hydrothermal synthesis and electrochemical properties. *Ceram. Int.* **2015**, *41*, 7556–7564. [[CrossRef](#)]
22. Hu, X.; Huang, H.; Zhang, J.; Shi, J.; Zhu, S.; Su, N. Controllable hydrothermal-assisted synthesis of mesoporous Co_3O_4 nanosheets. *RSC Adv.* **2015**, *5*, 99899–99906. [[CrossRef](#)]
23. Deloed, W.; Wattanathana, W.; Jantaratana, P.; Prompinit, P.; Wannapaiboon, S.; Singkammo, S.; Sattayaporn, S.; Laobuthee, A.; Suramitr, S.; Hanlumyuang, Y. A systematic variation in cationic distribution and its influence on the magnetization of mixed-metal (nickel and zinc) cobaltite spinels. *Mater. Res. Express* **2020**, *7*, 096104. [[CrossRef](#)]
24. Cao, X.; Yang, Y.; Li, A. Facile Synthesis of Porous ZnCo_2O_4 Nanosheets and the Superior Electrochemical Properties for Sodium Ion Batteries. *Nanomaterials* **2018**, *8*, 377. [[CrossRef](#)] [[PubMed](#)]
25. Wang, Y.; Li, J.; Chen, S.; Li, B.; Zhu, G.; Wang, F.; Zhang, Y. Facile preparation of monodisperse NiCo_2O_4 porous microcubes as a high capacity anode material for lithium ion batteries. *Inorg. Chem. Front.* **2017**, *5*, 559–567. [[CrossRef](#)]

26. Cook, D.S.; Wu, Y.; Lienau, K.; Moré, R.; Kashtiban, R.J.; Magdysyuk, O.V.; Patzke, G.R.; Walton, R.I. Time-Resolved Powder X-ray Diffraction of the Solvothermal Crystallization of Cobalt Gallate Spinel Photocatalyst Reveals Transient Layered Double Hydroxides. *Chem. Mater.* **2017**, *29*, 5053–5057. [[CrossRef](#)]
27. Moorhouse, S.J.; Wu, Y.; Buckley, H.C.; O'Hare, D. Time-resolved in situ powder X-ray diffraction reveals the mechanisms of molten salt synthesis. *Chem. Commun.* **2016**, *52*, 13865–13868. [[CrossRef](#)]
28. Philippot, G.; Boejesen, E.D.; Elissalde, C.; Maglione, M.; Aymonier, C.; Iversen, B.B. Insights into $\text{BaTi}_{1-y}\text{Zr}_y\text{O}_3$ ($0 \leq y \leq 1$) Synthesis under Supercritical Fluid Conditions. *Chem. Mater.* **2016**, *28*, 3391–3400. [[CrossRef](#)]
29. Chen, J.; Weidner, D.J.; Parise, J.B.; Vaughan, M.T.; Raterron, P. Observation of Cation Reordering during the Olivine-Spinel Transition in Fayalite by In Situ Synchrotron X-ray Diffraction at High Pressure and Temperature. *Phys. Rev. Lett.* **2001**, *86*, 4072–4075. [[CrossRef](#)]
30. Mittal, J. Recent progress in the synthesis of Layered Double Hydroxides and their application for the adsorptive removal of dyes: A review. *J. Environ. Manag.* **2021**, *295*, 113017. [[CrossRef](#)]
31. Karmakar, A.; Karthick, K.; Sankar, S.S.; Kumaravel, S.; Madhu, R.; Kundu, S. A vast exploration of improvising synthetic strategies for enhancing the OER kinetics of LDH structures: A review. *J. Mater. Chem. A* **2020**, *9*, 1314–1352. [[CrossRef](#)]
32. Chaillot, D.; Bennici, S.; Brendlé, J. Layered double hydroxides and LDH-derived materials in chosen environmental applications: A review. *Environ. Sci. Pollut. Res.* **2020**, *28*, 24375–24405. [[CrossRef](#)]
33. Kim, N.-I.; Sa, Y.J.; Yoo, T.S.; Choi, S.R.; Afzal, R.A.; Choi, T.; Seo, Y.-S.; Lee, K.-S.; Hwang, J.Y.; Choi, W.S.; et al. Oxygen-deficient triple perovskites as highly active and durable bifunctional electrocatalysts for oxygen electrode reactions. *Sci. Adv.* **2018**, *4*, eaap9360. [[CrossRef](#)] [[PubMed](#)]
34. Song, H.J.; Yoon, H.; Ju, B.; Kim, D. Highly Efficient Perovskite-Based Electrocatalysts for Water Oxidation in Acidic Environments: A Mini Review. *Adv. Energy Mater.* **2021**, *11*, 2002428. [[CrossRef](#)]
35. Xue, Y.; Sun, S.; Wang, Q.; Dong, Z.; Liu, Z. Transition metal oxide-based oxygen reduction reaction electrocatalysts for energy conversion systems with aqueous electrolytes. *J. Mater. Chem. A* **2018**, *6*, 10595–10626. [[CrossRef](#)]
36. Dai, Y.; Yu, J.; Ni, M.; Shao, Z. Rational design of spinel oxides as bifunctional oxygen electrocatalysts for rechargeable Zn-air batteries. *Chem. Phys. Rev.* **2020**, *1*, 011303. [[CrossRef](#)]
37. Priamushko, T.; Guillet-Nicolas, R.; Yu, M.; Doyle, M.; Weidenthaler, C.; Tüysüz, H.; Kleitz, F. Nanocast Mixed Ni–Co–Mn Oxides with Controlled Surface and Pore Structure for Electrochemical Oxygen Evolution Reaction. *ACS Appl. Energy Mater.* **2020**, *3*, 5597–5609. [[CrossRef](#)]
38. Veerabhadrapa, M.G.; Maroto-Valer, M.M.; Chen, Y.; Garcia, S. Layered Double Hydroxides-Based Mixed Metal Oxides: Development of Novel Structured Sorbents for CO_2 Capture Applications. *ACS Appl. Mater. Interfaces* **2021**, *13*, 11805–11813. [[CrossRef](#)]
39. Manohara, G.V.; Norris, D.; Maroto-Valer, M.M.; Garcia, S. Acetate intercalated Mg–Al layered double hydroxides (LDHs) through modified amide hydrolysis: A new route to synthesize novel mixed metal oxides (MMOs) for CO_2 capture. *Dalton Trans.* **2021**, *50*, 7474–7483. [[CrossRef](#)]
40. Maksoud, M.I.A.A.; Fahim, R.A.; Shalan, A.E.; Elkodous, M.A.; Olojede, S.O.; Osman, A.I.; Farrell, C.; Al-Muhtaseb, A.H.; Awed, A.S.; Ashour, A.H.; et al. Advanced materials and technologies for supercapacitors used in energy conversion and storage: A review. *Environ. Chem. Lett.* **2020**, *19*, 375–439. [[CrossRef](#)]
41. Chen, D.; Chen, C.; Baiyee, Z.M.; Shao, Z.; Ciucci, F. Nonstoichiometric Oxides as Low-Cost and Highly-Efficient Oxygen Reduction/Evolution Catalysts for Low-Temperature Electrochemical Devices. *Chem. Rev.* **2015**, *115*, 9869–9921. [[CrossRef](#)]
42. Kangvansura, P.; Schulz, H.; Suramitr, A.; Poo-Arporn, Y.; Viravathana, P.; Worayingyong, A. Reduced cobalt phases of ZrO_2 and Ru/ZrO_2 promoted cobalt catalysts and product distributions from Fischer–Tropsch synthesis. *Mater. Sci. Eng. B* **2014**, *190*, 82–89. [[CrossRef](#)]
43. Wannapaiboon, S.; Schneemann, A.; Hante, I.; Tu, M.; Epp, K.; Semrau, A.L.; Sternemann, C.; Paulus, M.; Baxter, S.; Kieslich, G.; et al. Control of structural flexibility of layered-pillared metal-organic frameworks anchored at surfaces. *Nat. Commun.* **2019**, *10*, 346. [[CrossRef](#)] [[PubMed](#)]
44. Poo-Arporn, Y.; Palangsuntikul, R. In Situ X-ray Absorption Near Edge Structure Study of Amorphous- TiO_2 Phase Transformation. *J. Nanosci. Nanotechnol.* **2016**, *16*, 6551–6554. [[CrossRef](#)] [[PubMed](#)]
45. Poo-Arporn, Y.; Chirawatkul, P.; Saengsui, W.; Chotiwan, S.; Kityakarn, S.; Klinkhieo, S.; Hormes, J.; Songsiririthigul, P. Time-resolved XAS (Bonn-SUT-SLRI) beamline at SLRI. *J. Synchrotron Radiat.* **2012**, *19*, 937–943. [[CrossRef](#)] [[PubMed](#)]
46. Wei, T.-Y.; Chen, C.-H.; Chien, H.-C.; Lu, S.-Y.; Hu, C.-C. A Cost-Effective Supercapacitor Material of Ultrahigh Specific Capacitances: Spinel Nickel Cobaltite Aerogels from an Epoxide-Driven Sol-Gel Process. *Adv. Mater.* **2010**, *22*, 347–351. [[CrossRef](#)]
47. Castorina, E.; Ingall, E.D.; Morton, P.L.; Tavakoli, D.A.; Lai, B. Zinc K-edge XANES spectroscopy of mineral and organic standards. *J. Synchrotron Radiat.* **2019**, *26*, 1302–1309. [[CrossRef](#)]
48. Ha, D.-H.; Moreau, L.M.; Honrao, S.; Hennig, R.G.; Robinson, R.D. The Oxidation of Cobalt Nanoparticles into Kirkendall-Hollowed CoO and Co_3O_4 : The Diffusion Mechanisms and Atomic Structural Transformations. *J. Phys. Chem. C* **2013**, *117*, 14303–14312. [[CrossRef](#)]
49. Smart, E.L.; Moore, E.A. *Solid State Chemistry: An Introduction*, 4th ed.; CRC Press: Boca Raton, FL, USA, 2012.
50. West, A.R. *Solid State Chemistry and Its Applications*, 2nd ed.; John Wiley & Sons: Chichester, UK, 2014.

-
51. Johnsen, R.E.; Norby, P. A comparative in situ Rietveld refinement study: Thermal decomposition and transformation of CoAl and CoZnAl layered double hydroxides. *J. Appl. Crystallogr.* **2008**, *41*, 991–1002. [[CrossRef](#)]
 52. Furnish, M.D.; Bassett, W.A. Investigation of the mechanism of the olivine-spinel transition in fayalite by synchrotron radiation. *J. Geophys. Res. Space Phys.* **1983**, *88*, 10333–10341. [[CrossRef](#)]